Defence Science Journal, Vol. 67, No. 2, March 2017, pp. 149-153, DOI : 10.14429/dsj.67.11178

Demonstration of Fabricated Midwave Infrared InAs/GaSb Type-II Superlattice-based Focal Plane Arrays

K.C. Goma Kumari, H.M. Rawool, and S. Chakrabarti*

Department of Electrical Engineering, Indian Institute of Technology Bombay, Mumbai - 400 076, India
**E-mail: subhanandachakrabarti@gmail.com*

ABSTRACT

In this study, fabricated 320 × 256 infrared focal plane arrays (FPAs) were realised using a GaSb/InAs-based type-II superlattice heterostructure for midwave infrared (MWIR) imaging. We report here the optimised fabrication and characterisation of single-pixel infrared detectors and FPAs. MWIR spectral response up to 5 µm of these single-pixel detectors was evident up to 250 K. Responsivity was measured to be 1.62 A/W at 0.8 V and 80 K. Current–voltage characteristics at room temperature (300 K) and at low temperature (18 K) revealed the resistance and dark current variation of the device in the operating bias region. Moreover, good thermal images were obtained at device temperatures up to 150 K for low-temperature targets. Low noise equivalent difference in temperature was measured to be 58 mK at 50 K and 117 mK at 120 K.

Keywords: Fabrication; Midwave infrared; Type-II superlattice; Focal plane array; FPA

1. INTRODUCTION

InAs/GaSb-based type-II superlattice (T2SL) midwave infrared (MWIR) detectors are used in applications such as medical diagnostics, night vision, and in security and defence devices[1]. The photocurrent responses of T2SL devices are significant, even at high temperatures (> 200 K); hence, these devices are also known as high operating temperature detectors[2,3]. Operations at high temperatures reduce cryogenic cooling costs[2,3]. Focal plane arrays (FPAs) with high operating temperatures of up to 170 K have also been demonstrated[4]. T2SLs are advantageous because their band-gap energy can be tailored to achieve cutoff wavelengths of up to 28 µm by varying the thickness of the InAs/GaSb layers[5].

In this paper, we report the optimised fabrication and characterisation of T2SL single-pixel detectors as well as the successful realisation of an FPA. The main challenge in developing high-performance T2SL FPAs is the use of passivation layer for reducing the surface leakage current[6]. Surface leakage current paths are formed because of the formation of unsatisfied bonds at the edges of the mesa wall during etching as well as the formation of conductive oxides, which degrades device performance, especially when the detector area is decreased, such as in FPAs[6]. Among the many passivation techniques, SU-8 polymer spinning is used as the surface passivation layer for FPA in this study[10,11].

2. DEVICE FABRICATION AND CHARACTERISATION

2.1 Heterostructure

Figure 1 illustrates the growth schematic of the procured pBiBn MWIR heterostructure on the basis of which the single-pixel detectors and FPAs were fabricated. The non intentionally doped (n.i.d) intrinsic absorber layer consists of 292 periods of 8 monolayers (MLs) of InAs and 8 MLs of GaSb with a total thickness of approximately 1.5 µm. Barrier layers on both sides of the absorber layer prevent the diffusion of minority carriers from the contact into the absorber layer and thus considerably reduce the dark current noise. The InAs/AlSb layer above the absorber layer forms a valence band offset, whereas the AlGaSb layer below the absorber layer forms a conduction band offset in order to prevent the flow of charge carriers from the contact to the absorber layer. 545 nm of p-type SLS forms

Figure 1. Schematic of the MWIR pBiBn heterostructure.

Received : 16 June 2016, Revised : 15 August 2016
Accepted : 21 December 2016, Online published : 11 March 2017

bottom contact and 20 nm n-type forms the top contact layers. Doping concentration in both the n-type and p-type contact layer is 2×10^{18} cm^3.

2.2 Single-Pixel Device Fabrication

The mesa and metal masks used for fabricating single-pixel devices comprise round and square single pixels of optical aperture sizes varying from 50 µm to 600 µm. First, the mesa resist was patterned using the mesa mask onto the sample by spin-coating a positive photoresist (SPR700), exposing to UV radiation on a double-sided aligner (DSA), and developing in MF319 developer. Subsequently, the resist was hardened through post-baking so that it can withstand wet etching. The wet-etching recipe was optimised by examining the effect of different proportions of citric acid (citric acid monohydrate: water = 1:1 by weight), phosphoric acid, hydrogen peroxide, and deionised water ($CA:H_3PO_4:H_2O_2:H_2O$) on dummy substrates[7]. The optimal ratio was found to be 4:1.25:2:20, which yielded a smooth surface and better etch profile at an etch rate of approximately 380 nm/min. The sample was etched for approximately 390s to an etch depth plus resist thickness of nearly 4.5 µm, as measured by a stylus profilometer, to ensure that the p+ SLS bottom contact layer is reached, after etching through the AlGaSb layer. The final mesa height was measured to be 2.5 µm, which was within the target etch depth range. Figure 2(a) presents the images of the mesa after etching and removing the photoresist.

Similarly second-level lithography was performed to open windows on resist mask for depositing the top and bottom metal contacts (Fig. 2(b)). To form an ohmic contact, a Ti (40 nm)/Au (200 nm) metal stack was deposited using a six target electron beam evaporator, following which the resist was lifted[8,9]. The formation of the ohmic contact was confirmed by measuring the I–V characteristics between the bottom to bottom contact by a probe station. The sample was then diced and fixed in a leadless chip carrier (LCC) by using epoxy for characterisation at various temperatures (18 K – 300 K). The contacts were wire bonded to the LCC pads by using a semiautomatic wire bonder system with 25 µm gold wires, according to the wiring scheme of the cryostat used for various characterisations.

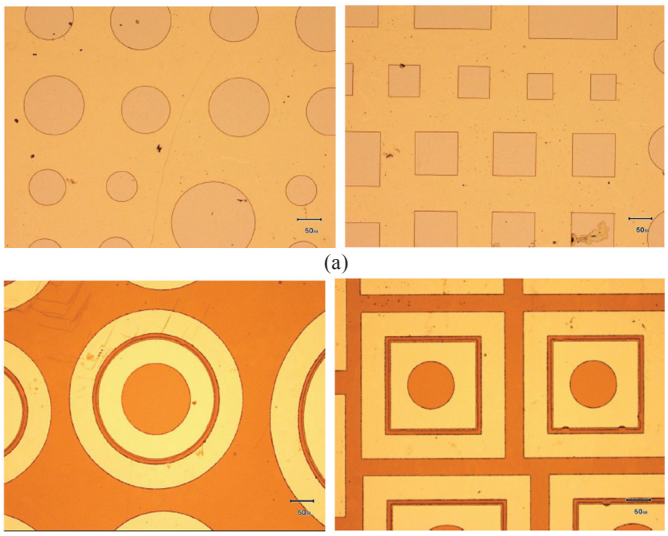

Figure 2. (a) Mesa images after etching and resist removal and (b) Metal contact window after second-level lithography.

2.3 Single-Pixel Device Characterisation

The single-pixel detectors fixed to the LCCs were mounted on the cold finger of the closed-cycle liquid-helium cryostat (temperature range: 18 K – 300 K). A cold shield was installed when measuring the dark current. The system was pumped down to the lowest possible temperature, following which we measured the current–voltage (I–V) characteristics at both low temperature (18 K) and room temperature (300 K) by using a Keithley source meter 2400 connected to a computer. A custom LabVIEW Code was used to program the source meter to scan from − 2 V to + 2 V, and the corresponding current was acquired and plotted.

For other photo response measurements, the system was warmed and the cold shield repositioned so that the test IR radiation fell on the detector. The system was cooled again and placed 14 cm away from a blackbody calibration source (900 K) with an aperture of 12.5 mm. An optical chopper, operated at 275 Hz, was placed between the source and the detector. The device was biased using a Keithley 428 current amplifier, and its output was measured using a network analyser (SR760, Stanford Research Systems). Blackbody responsivity was calculated as $R = A/(E \times A_d)$, where A is the photocurrent, E is the incident radiation (after accounting for cryostat window transmission losses and the chopping factor), and A_d is the device aperture area. Responsivity measurement as a function of bias gave an idea of operating bias range of the FPA fabricated from the same substrate and the suitability of the ROIC.

Spectral response was measured using a broadband IR source Fourier transform IR spectrometer (FTIR; IS50R, Thermo Fisher). The photo response signal from the current preamplifier was fed back to the FTIR auxiliary input so that the spectrometer's native Omnic software could plot the spectral response. The plotted response was normalised against the response from its internal detector.

2.4 FPA Fabrication

The mask set for the 320 × 256 FPA has a mesa of size 24 µm × 24 µm (pitch = 30 µm). Similar to the procedure for single-pixel device fabrication, mesa lithography and etching were performed (Fig. 3(a)) for the FPA. After wet etching and resist removal, the device was immediately cleaned and passivated using spinning SU8 polymer; subsequently, the device was spin coated and loaded on the DSA and exposed to UV radiation along with corresponding mask plate to create a 15 µm × 15 µm opening. Then, the device was developed and hard baked, thus making it a permanent structure. Next, Under Bump Metal (UBM) contact lithography was performed, and a Ti/Au stack was deposited using the metal evaporator system (Fig. 3(b)). Finally, 2.2-µm-thick indium bump pads were deposited through lithography (Fig. 3(c)).

The indium was reflowed on a hot plate at 200 ºC for approximately 60 s with water-soluble reflow flux to facilitate the formation of indium bumps by increasing the surface tension of the molten indium. The flux was then cleaned before

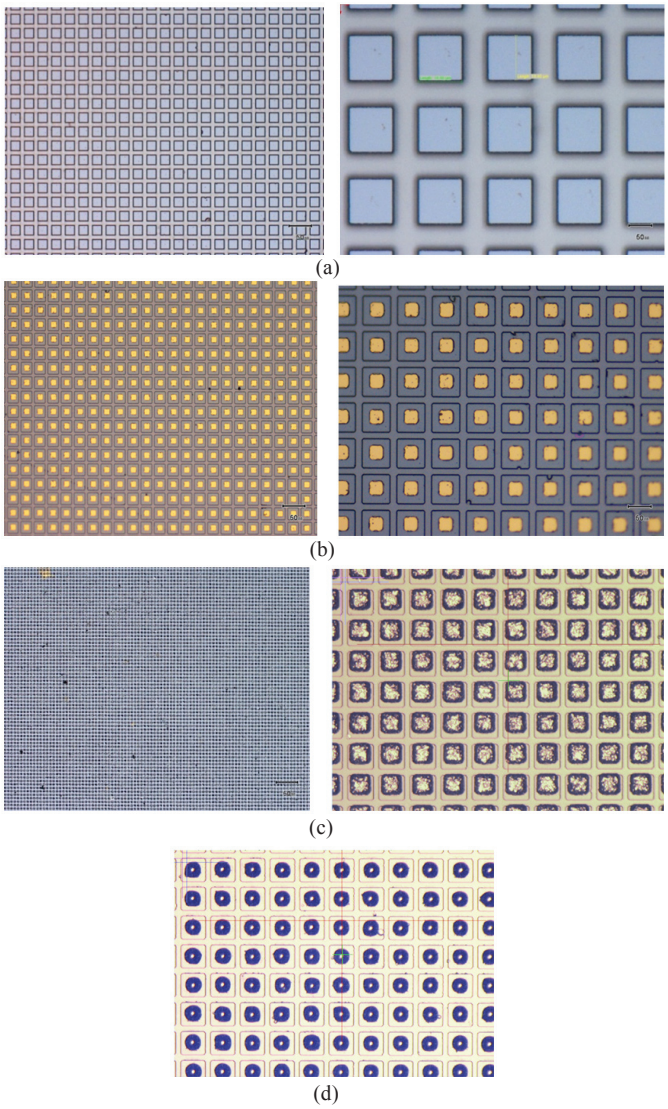

Figure 3. (a) FPA mesa, (b) FPA UBM, (c) Indium bump pads in the FPA, and (d) FPA after reflow.

flipchip bonding. Next, the FPA was hybridised on to a IS9705 Si read-out integrated circuit (ROIC) at 205 ºC by using a SET FC150 bonder. The gap between the FPA device and the ROIC was filled with underfill (Henkel Hysol) and cured to impart the mechanical strength necessary to withstand mechanical lapping and to reduce fatigue. FPAs are back-illuminated devices; hence, most of the substrate was removed by mechanical lapping, polishing, and chemical etching to a final device thickness of approximately 40 µm. Moreover, device thinning reduces the probability of stress-induced cracking caused by the mismatch between the thermal expansion coefficients of Si ROIC and the FPA device at low temperatures. Further, thinner devices can withstand temperature cycling fatigue.

2.5 FPA Imaging

The FPA was fixed on a LCC and the corresponding pins on the ROIC are wire-bonded according to the internal electronic board of the CamIRa (SEIR) setup. The CamIRa system is equipped with a single-stage closed-cycle liquid-helium cryostat that can cool the FPA to 50 K. It has a modular bias and clock cards and was configured for FPAs hybridised on to 9705 ROICs. The system was fitted with an imaging lens of focal length 50 mm and has a wide passband of 3 µm – 12 µm. An extended blackbody source was used as the reference target to measure the low noise equivalent difference in temperature (NEΔT) and to perform non-uniformity correction before capturing test images of human subjects.

The spectral response from the FPA was measured using the FTIR interferometer through the step-scan technique, wherein the IR source output was focused on the FPA by using a gold-coated parabolic mirror. Mirror movement in the FTIR interferometer and data acquisition in the CamIRa setup was synchronised, and the interferogram was reconstructed and inverse Fourier transformed using a custom LabVIEW code to obtain the spectral response.

3. RESULTS AND DISCUSSION

Figure 4 presents bias-dependent dark currents measured at device temperatures of 18 K – 300 K, and Fig. 5 presents the temperature-dependent spectral response curve at V = 0.8 V. The device exhibited a broad spectral response in the mid-wavelength range (1.8 µm – 5 µm). As the device temperature

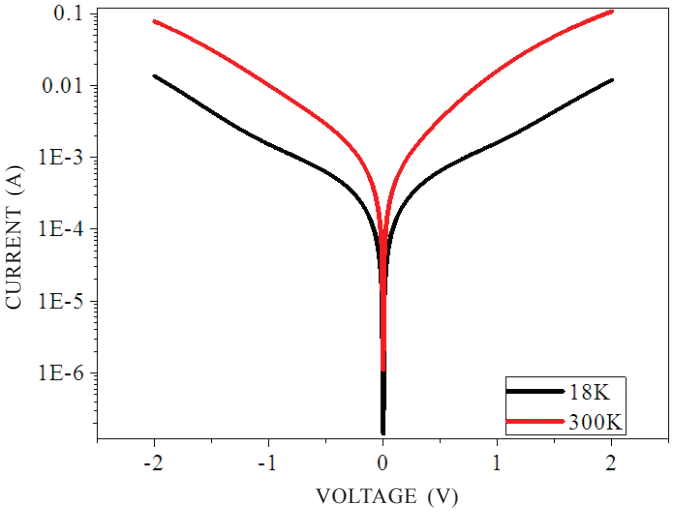

Figure 4. I–V curves at 18 and 300 K.

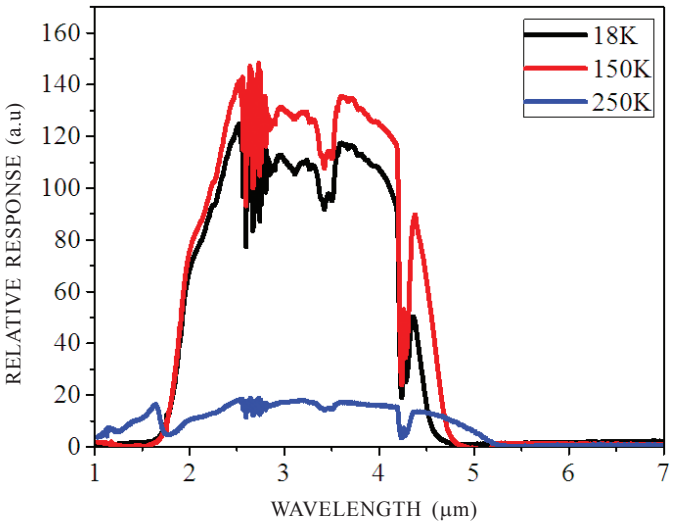

Figure 5. Spectral response at different temperatures.

was increased, the response tail shifted to longer wavelengths. At 18 K, the response was up to 4.5 µm, whereas at 150 and 250 K, it extended to 4.7 µm and 5.2 µm, respectively. Sharp dips in the spectrum are from atmosphere absorption (H_2O and mainly CO_2) bands. Figure 6 shows the responsivity plot as a function of the bias voltage; the responsivity measured at 0.8 V and 80 K was 1.62 A/W. The response is significant at positive bias, whereas no response is observed at negative bias and hence the FPA is operated at positive bias.

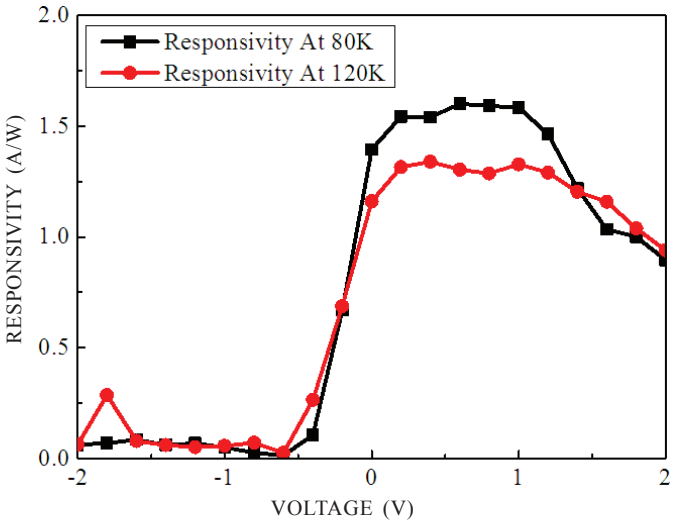

Figure 6. Responsivity at 80 and 120 K.

Figure 7 depicts the spectral response of the FPA measured through the aforementioned step-scan technique. The FPA response agrees well with that obtained from single-pixel devices.

Figure 8 presents the thermal images of human faces generated using the FPA at 50 K – 150 K. Hotter targets could be imaged even at operation temperatures exceeding 150 K. For example, we successfully imaged a heat gun (temperature:

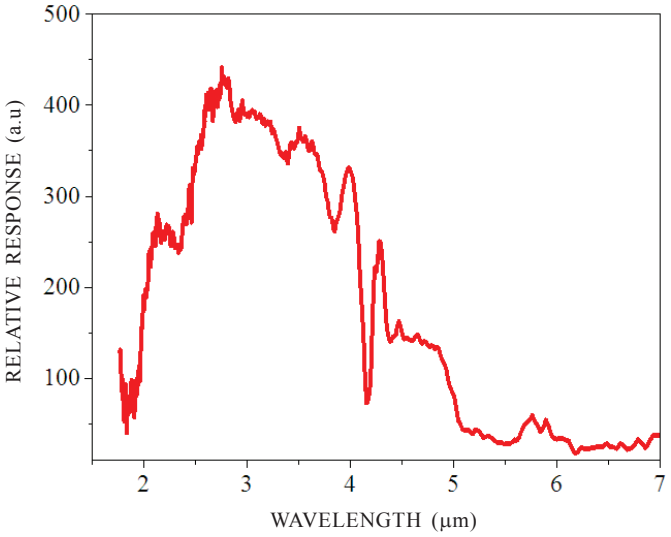

Figure 7. Spectral response of FPA at V = 0.5 V and T = 50 K.

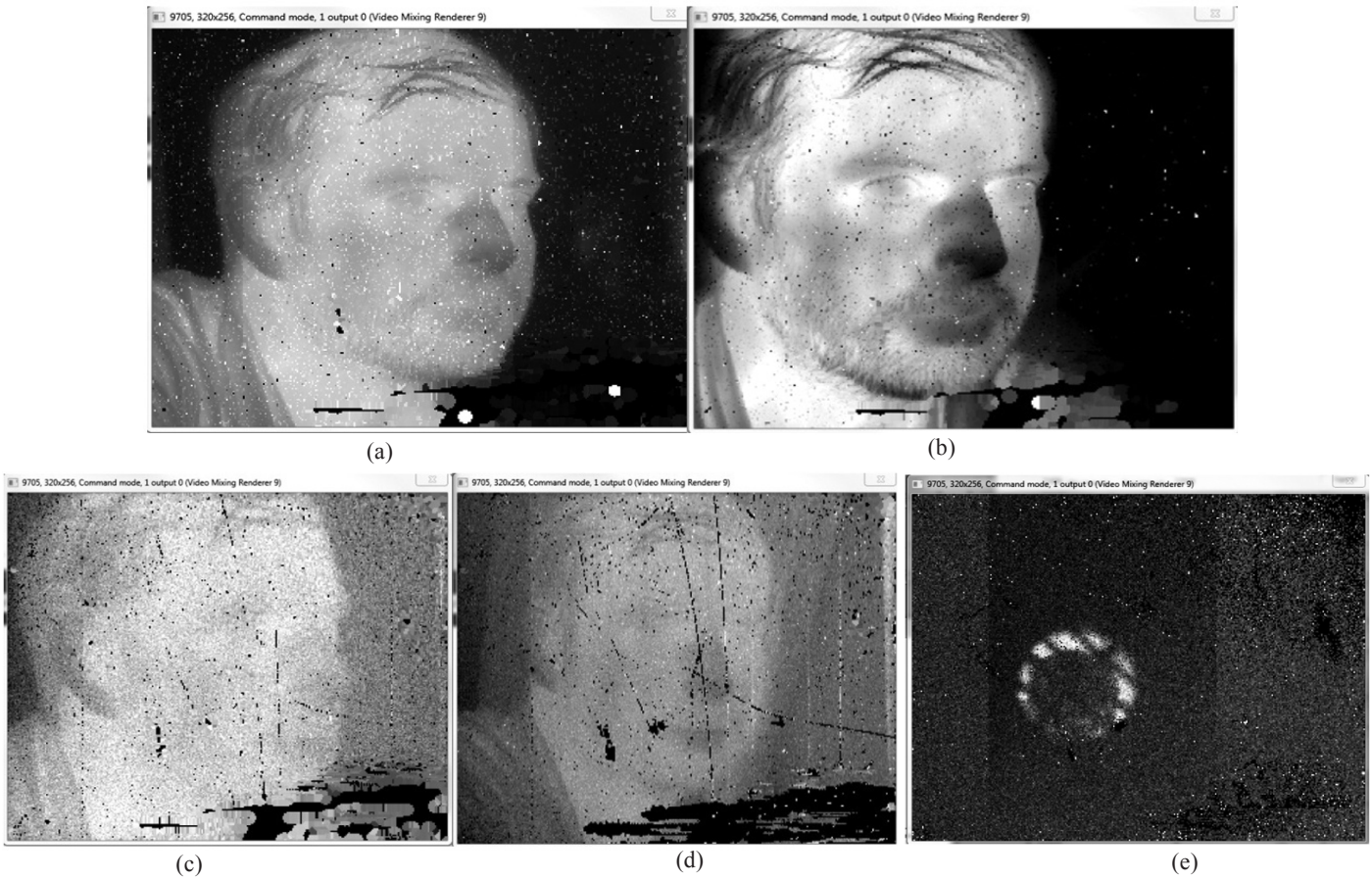

Figure 8. FPA images captured at (a) 50 K, (b) 80 K, (c) 120 K, and (d) 150 K; (e) image of the heat gun at an FPA temperature of 300 K.

350 ºC – 400 ºC) by using the FPA at room temperature (300 K). NEΔT measured at various FPA temperatures is listed in Table 1. We measured NEΔT values of 58 mK and 117 mK at FPA temperatures of 50 K and 120 K, respectively.

Table 1. Measured NEΔT for the fabricated FPA.

FPA Temperature (K)	NEΔT at 25 °C (mK)
50	58
70	91
80	98
120	117
130	498
140	1364
150	3101

4. CONCLUSIONS

We report the successful fabrication and characterisation of single-pixel MWIR T2SL InAs/GaSb-based detectors. The highest measured responsivity was 1.62 A/W. To the best of our knowledge, we have successfully fabricated and demonstrated the first InAs/GaSb-based T2SL MWIR 320 × 256 FPA in India, which could image human targets even at higher operating temperatures (i.e. up to 150 K). Moreover, this T2SL FPA exhibits room temperature operation for higher temperature targets (> 300 ºC).

REFERENCES

1. Rogalski, A. & Martyniuk P. InAs/GaInSb superlattices as a promising material system for third generation infrared detectors. *Infrared Phys. Technol*., 2006, **48**(39). doi:10.1016/j.infrared.2005.01.003.
2. Sai-Halasz, G.A.; Tsu, R.; & Esaki, L. A new semiconductor superlattice. *Appl. Phys. Lett.*, 1977, **30**, 651-653. doi: 10.1063/1.89273.
3. Smith, D.L. & Mailhiot, C. Proposal for strained type-II superlattice infrared detectors. *J. Appl. Phys.*, 1987, **62**, 2545-2548. doi: 10.1063/1.339468.
4. Razeghi, M.; Abdollahi, S.P.; Huang, E.; Chen, G.; Haddadi, A. & Nguyen, V. Type-II InAs/GaSb photodiode and focal plane arrays aimed at high operating temperatures. *Opto-Electronics Rev.*, 2011, **19**, 261-269. doi: 10.2478/s11772-011-0028-0.
5. Gautam, N.; Myers, S.; Barve, A.V.; Klein, B.; Smith, E.P.; Rhiger, D.; Plis, E.; Kutty, M.N.; Henry, N.; Schuler-Sandy, T. & Krishna, S. Band engineered HOT midwave infrared detectors based on type-II InAS/GaSb strained layer superlattice. *Infrared Phys. Technol.*, 2013, **59**, 72-77. doi:10.1016/j.infrared.2012.12.017.
6. Tan, S.L.; Goh, Y.L.; Das, S.D.; Tan, C.H.; David, J.P.R.; Gautam, N.; Kim, H.; Plis, E. & Krishna, S. Dry etching and surface passivation techniques for type-II InAs/GaSb superlattice infrared detectors. *In* Proc. of SPIE, **7838**, 783814-1. doi: 10.1117/12.864787.
7. Kowalewski, A.; Martyniuk, P.; Markowska, O.; Benyahia, D. & Gawron, W. New wet etching solution molar ratio for processing T2SLs InAs/GaSb nBn MWIR infrared detectors grown on GaSb substrate. *Mater. Sci. Semiconductor Proces.*, 2016, **41**, 261-264. doi: 10.1016/j.mssp.2015.08.034.
8. Kim, H.S.; Mayers, S.; Klein, B.; Kazemi, A. & Krishna, S. Dark current improvement of the type-II InAs/GaSb superlattice photodetectors by using a gate bias control. *J. Korean Phys. Society*, 2015, **66**(4). doi: 10.3938/jkps.66.535.
9. Tian, Z.; DeCuir Jr., E.A.; Wijewarnasuriya, P.S.; Pattison, J.W.; Gautam, N.; Krishna, S.; Dhar, N.; Welser, R.E. & Sood, A.K. Low dark current structures for long wavelength type-II strained layer superlattice photodiodes. *Proc. of SPIE*, **8704**, 870415-1. doi: 10.1117/12.2015489.
10. Henry, N.C.; Knorr Jr., D.B.; Williams, K.S.; Baril, N.; Nallon, E.; Lenhart, J.L.; Andzelm, J.W.; Pellegrino, J.; Tidrow, M.; Cleveland, E. & Bandara, S. Chemical and physical passivation of type-II strained –layer superlattice device by means of thiolated self-assembled monolayer and polymer encapsulates. *Infrared Phys. Technol.*, 2015, **70**, 48-52. doi: 10.1016/j.infrared.2014.10.015.
11. Plis, E.; Kutty, M.N.; Mayers, S.; Kim, H.S.; Gautam, N.; Dawson, L.R. & Krishna, S. Passivation of long-wave infrared InAs/GaSb strained layer superlattice detectors. *Infrared Phys. Technol.*, 2011, **54**, 252-257. doi: 10.1016/j.infrared.2010.12.024.

ACKNOWLEDGMENTS

We acknowledge the financial support received from Defence Research and Development Organisation, India. Partial funding from the Department of Science and Technology, India, ISRO India as well as from Indian Institute of Technology Bombay Nanofabrication Facility (IITBNF) are also being acknowledged.

CONTRIBUTORS

Ms K.C. Goma Kumari received her MSc (Analytical Chemistry) from SNDT University, Mumbai, in 2011. She has since been assisting a research group in the Department of Electrical Engineering at Indian Institute of Technology (IIT) Bombay. She is involved in the fabrication and characterisation of III–V detectors.

Mr H.M. Rawool received his BE (Instrumentation) from University of Mumbai, India, in June 2012. After graduation, he joined a research group at IIT Bombay in July 2012, where he is currently pursuing his master's. He is involved in fabricating and characterising III–V group single pixel detectors.

Dr S. Chakrabarti received his MSc and PhD from the Department of Electronic Science, University of Calcutta, Kolkata, India, in 1991 and 2000, respectively. Presently, he is a professor in the Department of Electrical Engineering, IIT Bombay, Mumbai, India. He has extensively researched molecular beam epitaxial growth, characterisation, and fabrication of compound (III–V) GaAs-based semiconductor optoelectronic materials and devices. In II–VI ZnO-based research, he has demonstrated stable p-doping through plasma immersion ion implantation as well as a homojunction ZnO-based UV-LED.